Multi-criteria geometric optimization of a radial-flow adsorber for direct air capture

Konstantin Zaynetdinov*, Eero Inkeri, Payman Jalali, Tero Tynjälä

Lappeenranta-Lahti University of Technology LUT, Lappeenranta, Finland
** Corresponding author: konstantin.zaynetdinov@lut.fi*

Abstract:

Direct air capture (DAC) is expected to play an important role in achieving net-zero targets, but its wider deployment is limited by high cost and energy demand. Improving the process efficiency and equipment design at all steps of the DAC process is critical for its implementation. This work focuses on geometric optimization of a radial-flow adsorber for DAC based on a solid adsorbent, aiming to improve the adsorption stage and the overall unit performance. Several configurations of an adsorber are investigated and the adsorption stage of DAC is simulated using computational fluid dynamics (CFD). The CFD model uses source terms to simulate the adsorption of carbon dioxide from air based on the linear driving force model, and the adsorption bed is treated as a non-isothermal porous medium. The specific energy requirement and the productivity of the adsorption stage are compared across all configurations, while taking into consideration the capital cost indicators and space requirements. Multi-criteria optimization methods are applied to rank and select preferable configurations depending on the relative importance assigned to the above-mentioned metrics. The results suggest that increasing the bed aspect ratio and the radius ratio of the adsorber reduces the specific energy requirement at the expense of higher capital costs and larger space requirements. Increasing the bed aspect ratio along with decreasing the radius ratio significantly reduces the productivity of the unit, which should be avoided. In summary, these results provide practical design guidance for radial-flow adsorbers in solid-sorbent DAC, enabling a balance between unit performance and deployment constraints when selecting an adsorber geometry.

Keywords:

Direct air capture; Radial-flow adsorber; Modeling; Optimization, Multi-criteria decision-making.

1. Introduction

Climate change and the ongoing increase in global temperature are already affecting natural and human systems, causing intense heatwaves, changes in precipitation patterns that increase the risk of both floods and droughts, and other harmful impacts. Carbon dioxide (CO_2) is the main contributor to long-term global warming because it is released in large amounts through human activities, especially fossil-fuel combustion and industrial processes [1]. Reducing CO_2 emissions is essential to limit the global temperature increase; however, total elimination of some emissions is challenging. That is why carbon dioxide removal (CDR) technologies play an important role in achieving net-zero emission targets [2].

Direct air capture (DAC) is a process by which CO_2 can be extracted from the ambient air. DAC technology with subsequent geological storage of CO_2 is a promising CDR technology because it offers a high potential for mitigation and durable storage of carbon dioxide [3]. It has a significantly smaller land footprint and lower water demand than other CDR approaches [4]. However, DAC remains among the most expensive and energy-intensive CDR approaches currently available, making improvements in process efficiency and equipment design essential across all stages of the process [3].

The use of sorbents that bind CO_2 from the air is central to DAC technology. The DAC sorbents are classified into solid and liquid sorbents. Extensive reviews on both solid and liquid sorbents for DAC can be found in [5-10]. This work addresses solid-sorbent DAC. Solid sorbents typically offer better sorption kinetics, avoid solvent evaporation and associated heat losses, and release less volatile components to the atmosphere [5,6]. Solid-sorbent DAC is more energy intensive; however, regeneration of solid sorbents is performed at lower

temperatures (80–100 °C), which can make integration with low-carbon heat sources more straightforward, whereas liquid systems involve higher-temperature (300–900 °C) regeneration conditions. Solid-sorbent DAC is also commonly designed in a modular way, enabling scale-up by adding parallel units. Liquid-solvent DAC is often associated with large-scale deployment and generally requires a continuous supply of water for operation [11]. Amine-functionalized sorbents are considered one of the most promising options for DAC as they show high CO_2 uptake and good selectivity at low CO_2 concentrations [7-10].

Fixed-bed columns are the most extensively investigated gas-solid contactors for DAC because of their straightforward and robust design. In these systems, the sorbent is retained as a stationary packed layer, and the gas is driven through that layer for mass transfer to occur. However, conventional fixed-bed columns often suffer from high pressure losses, which restrict feasible flow velocities and adsorbent particle sizes. For this reason, alternative fixed-bed geometries have been examined to reduce the flow resistance and provide a larger contact area, such as flat beds, structured beds, or radial-flow annular beds [4]. In radial-flow adsorbers, the adsorbent is placed in a concentric annular region between an inner pipe and an external annular channel, with the gas crossing the bed radially between these zones [12,13].

Radial-flow adsorbers can be classified into four basic configurations by combining two radial flow directions with two axial arrangements of inlet and outlet and the corresponding flow patterns. Specifically, centripetal and centrifugal describe whether the gas flows radially inward or outward through the bed, while Z-type and π-type indicate whether the inlet and outlet are positioned at the opposite ends or at the same end of the adsorber, respectively [14].

Computational fluid dynamics (CFD) modeling has been used in studies of adsorption-based CO_2 capture and DAC as a strong tool for optimizing device configurations and operating conditions. Several studies [15-17] have examined the conventional fixed-bed column geometry. Alternative configurations have also been investigated, including a W-shaped fixed-bed adsorber [18] and a cylindrical gyroid filter [19] for DAC, as well as a radial-flow adsorber for CO_2 capture [20]. CFD has also been applied to radial-flow adsorbers in other gas separation applications. For example, four types of radial-flow adsorbers were compared for binary adsorption of CO_2 and water [14]; geometric optimization was performed for both centripetal Z-type [21] and centripetal π-type [22] adsorbers. In some studies [19,21], only the gas flow was simulated without modeling the adsorption process but with a focus on predicting pressure drop and improving flow uniformity.

When adsorption is included in CFD simulations, the model must define how the mass transfer between the gas and solid phases (adsorption kinetics) and the equilibrium adsorption capacity are described. The linear driving force (LDF) model is the most common approach for adsorption kinetics modeling, while Langmuir-type adsorption isotherms are typically used to represent adsorption equilibrium. CFD simulations of adsorption also require assumptions for pressure drop and heat transfer in the porous bed. The Ergun equation is the most widely used pressure-drop model, while heat transfer can be treated either by an equilibrium model with a shared temperature for the gas and solid phases or by a non-equilibrium model that solves separate temperature fields for each phase. Reference [23] provides a more detailed review of modeling the adsorption-based CO_2 capture.

Despite the frequent use of CFD for detailed modeling of adsorption-based CO_2 capture, radial-flow adsorbers for DAC have not received much attention, even though they can improve the efficiency of the DAC process, and CFD modeling is a useful method for the optimization of such systems. The current work addresses this gap by using CFD to investigate the adsorption phase of a solid-sorbent DAC process in different configurations of a centripetal Z-type contactor. Several multi-criteria decision-making approaches are used to analyze the results and identify the optimal configuration.

2. Methods

A two-dimensional axisymmetric model of a radial-flow adsorber for DAC is developed in Ansys Fluent. The computational domain is divided into three regions as shown in Figure 1: an inflow channel, an adsorption bed and an axial outflow channel. The airflow enters from the outer side of the adsorbent region and passes through the bed in the radial direction toward the center of the device. The adsorption bed is treated as a porous medium. To enable a non-equilibrium porous-medium heat transfer model, the dual-cell approach is employed, where an overlapping solid domain coincident with the porous fluid region is defined.

The gas phase is assumed to be an ideal two-component mixture of nitrogen and carbon dioxide. The flow is considered laminar in all parts of the domain. Since CO_2 is present in the air at a very low concentration, removing it by adsorption does not significantly affect the flow in the device. For this reason, the flow is first solved using the steady-state continuity and momentum equations:

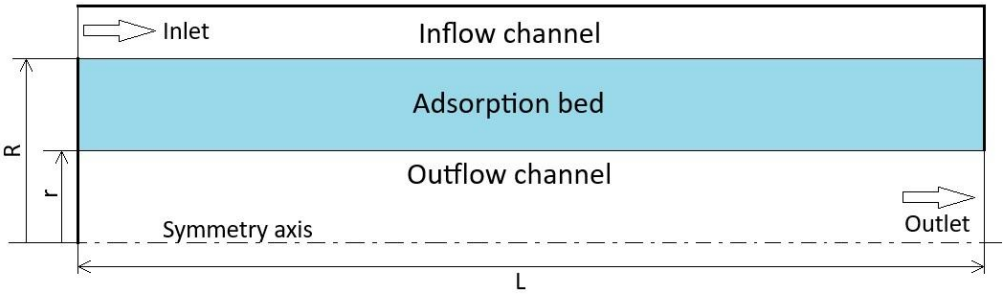

Figure 1. *Computational domain*

$$\nabla \cdot (\rho \vec{v}) = 0 \tag{1}$$

$$\nabla \cdot (\rho \vec{v}\vec{v}) = -\nabla p + \nabla \cdot \bar{\tau} - \left(\frac{\mu}{\alpha}\vec{v} + C_2 \frac{1}{2}\rho|\vec{v}|\vec{v}\right) \tag{2}$$

The last term in Eq. 2 represents the momentum sink due to flow resistance exerted by the porous medium. It is composed of the viscous and inertial loss terms. The permeability α [m^2] and the inertial resistance factor C_2 [m^{-1}] are calculated using the Ergun equation.

After obtaining the flow field, the transient simulations are performed. The mass fraction of CO_2 Y_{CO_2} in the gas phase is calculated from the species transport equation:

$$\frac{\partial}{\partial t}\left(\varepsilon \rho Y_{CO_2}\right) + \nabla \cdot \left(\rho \vec{v} Y_{CO_2}\right) = -\nabla \cdot \vec{J}_{CO_2} + S_{CO_2} \tag{3}$$

where $\vec{J}_{CO_2}$ is the diffusion flux,

$$\vec{J}_{CO_2} = \rho D_{m,CO_2} \nabla Y_{CO_2} \tag{4}$$

and S_{CO_2} is the CO_2 mass sink due to adsorption defined as

$$S_{CO_2} = -\frac{m_{ads} M_{CO_2}}{V_{cell}} \frac{\partial q}{\partial t} \tag{5}$$

The adsorption rate in Eq. 5 is calculated using the LDF model:

$$\frac{\partial q}{\partial t} = k_{LDF}\left(q_{eq} - q\right) \tag{6}$$

where k_{LDF} is the mass transfer rate coefficient [1/s], q_{eq} is the equilibrium adsorption capacity, and q is the current amount of adsorbed CO_2 per mass of adsorbent [mol_{CO2}/kg_{ads}]. The Toth isotherm model is used to calculate the equilibrium adsorption capacity. A commercial amine-functionalized adsorbent for DAC is taken as the basis for the material properties used in this model, including the Toth model parameters and the mass transfer coefficient.

Transient energy equations are solved for the fluid zones and solid porous zone coupled through the interphase heat transfer term in both equations:

$$\frac{\partial}{\partial t}(\varepsilon \rho_f E_f) + \nabla \cdot \left(\vec{v}(\rho_f E_f + p)\right) = \nabla \cdot \left(\varepsilon k_f \nabla T_f - h_{CO_2} \vec{J}_{CO_2}\right) + h_{fs} A_{fs}(T_s - T_f) + S_E \tag{7}$$

$$\frac{\partial}{\partial t}\left((1-\varepsilon)\rho_s E_s\right) = \nabla \cdot \left((1-\varepsilon) k_s \nabla T_s\right) + h_{fs} A_{fs}(T_f - T_s) \tag{8}$$

The source term in the energy equation (Eq. 7) represents the CO_2 enthalpy sink and the energy released during adsorption:

$$S_E = S_{\mathrm{CO_2}} \left(\bar{c_p}(T - T_{\mathrm{ref}}) - \frac{\Delta H}{M_{\mathrm{CO_2}}} \right) \tag{9}$$

The boundary conditions are presented in Figure 1. A constant mass flow rate, a temperature (20 °C) and a mass fraction of CO_2 (430 ppm) are defined for the inlet. A static pressure of 0 Pa is set for the outlet. The walls are adiabatic with no-slip boundary conditions for the flow equations. The initial conditions of 20 °C and zero CO_2 mass fraction are set for the entire domain. The simulations are performed with a time step of 0.1 s because the adsorption process takes place at a slow rate.

The geometric optimization study is performed by varying two geometric parameters: the bed aspect ratio (AR) and the radius ratio (RR), while keeping the volume of the bed the same. These parameters are defined as follows:

$$\mathrm{AR} = \frac{R - r}{L} \tag{10}$$

$$\mathrm{RR} = \frac{r}{R} \tag{11}$$

The reference case is defined using the following dimensions of the adsorber: $r = 0.06$ m, $R = 0.12$ m, $L = 0.48$ m, which gives $AR = 8$, $RR = 0.5$. A total of 12 cases are simulated with AR values of 4, 8, 16, 32, and RR values of 0.3, 0.5, 0.7. The dimensions of all configurations are given in Appendix A. The same inlet mass flow rate is used for all cases so that a pressure drop of 200 Pa is obtained in the reference case.

The mesh sensitivity study is performed for the reference case to ensure grid independence. Several meshes are created ranging from 4500 to 36000 cells. The pressure drop and the time needed to reach 95% saturation of the bed are compared between the meshes. As a result of the study, the mesh containing 18000 cells is selected, since a further increase of the number of cells does not noticeably improve the solution.

To evaluate the simulated cases and identify optimal configurations of the adsorber, multi-criteria decision-making approaches are applied. The main criteria that are considered in this study are specific energy requirement (SER) [J/kg_{CO2}] of adsorption, productivity [$kg_{CO2}/(kg_{ads}\ s)$], total surface area [m^2], and total volume [m^3] of the unit. Specific energy requirement is defined as the energy needed to adsorb one kilogram of CO_2 and is calculated as follows:

$$\mathrm{SER} = \frac{Q t_{\mathrm{sat}} \Delta p}{m_{\mathrm{CO2}}} \tag{12}$$

where Q [m^3/s] is the volumetric flow rate of the gas mixture, Δp [Pa] is the pressure drop, t_{sat} [s] is the time to reach 95% saturation of the bed, m_{CO2} [kg] is the mass of CO_2 adsorbed during the time t_{sat}.

Productivity is also defined based on the saturation time as the mass of CO_2 adsorbed per time per kilogram of adsorbent. Total surface area is included in the study because it represents the cost of the construction materials. The volume of the adsorber is considered as it affects the space requirements.

3. Results and discussion

The results of the CFD simulations are presented in Figure 2 and Table 1. Figure 2 shows the saturation of the bed during the adsorption process in all cases. As can be seen, the 95% saturation is achieved in all cases by 14 hours of adsorption except for the case of $AR = 32$, $RR = 0.3$. It can be calculated from Eqs. 10 and 11 that in this case, the inner pipe must be very long (1.42 m) and have a very small radius (1.9 cm) to keep the volume of the bed the same as in the reference case. These dimensions cause a very large pressure drop over the inner pipe which leads to high flow non-uniformity. As a result, a part of the bed remains unsaturated for a long time while CO_2 can already be detected at the outlet. This underutilzation of the bed should be avoided in the design of adsorbers, so this case is excluded from further analysis. The same phenomenon

causes slower saturation in the cases of $AR = 32$, $RR = 0.5$ and $AR = 16$, $RR = 0.3$, which results in reduced productivity, as can be seen from Table 1. The data in Table 1 also show that the pressure drop is the main factor affecting the SER since the saturation time does not change significantly, and other parameters in Eq. 12 are the same in all cases. The surface area increases with an increase in bed aspect ratio and radius ratio. If the bed volume is kept constant, the total volume depends only on the radius ratio of the unit.

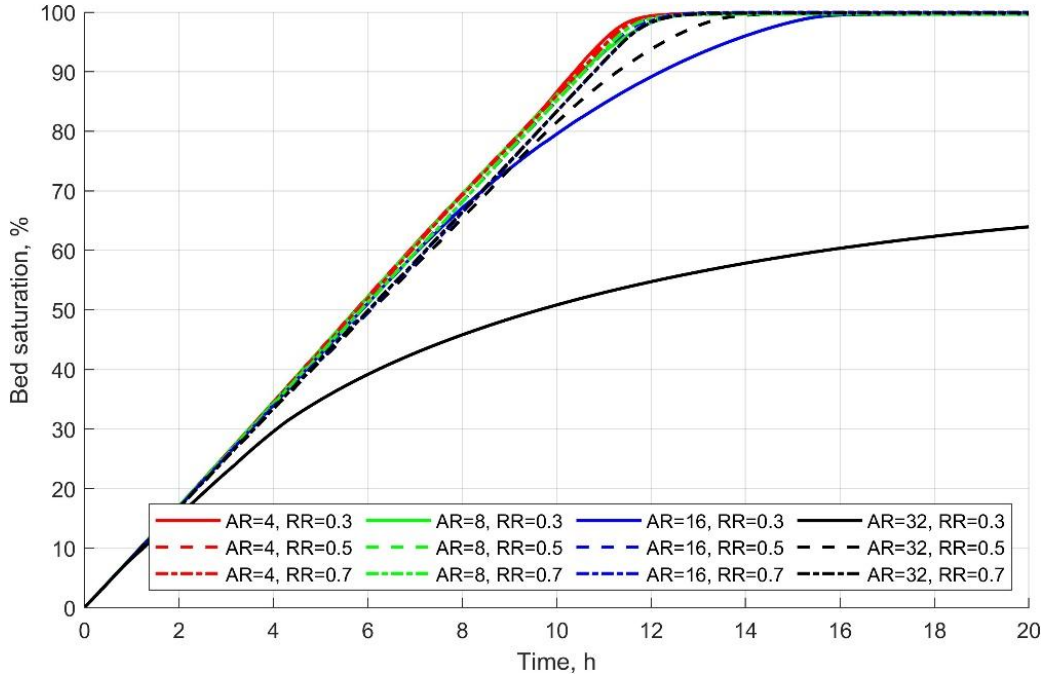

Figure 2. *Bed saturation during adsorption in all cases*

Table 1. *Main simulation results*

AR	RR	Pressure drop, Pa	Saturation time, h	SER, MJ/kg_{CO2}	Productivity, $g_{CO2}/(kg_{ads}$ h)	Surface area, m^2	Volume, liters
4	0.3	491.0	10.91	3.80	0.774	0.464	17.9
4	0.5	315.6	10.95	2.45	0.771	0.557	21.7
4	0.7	198.6	11.04	1.56	0.765	0.730	32.0
8	0.3	345.5	11.23	2.76	0.752	0.524	17.9
8	0.5	200.0	11.04	1.57	0.765	0.622	21.7
8	0.7	124.4	11.14	0.99	0.758	0.796	32.0
16	0.3	322.7	13.53	3.10	0.624	0.622	17.9
16	0.5	131.7	11.17	1.05	0.756	0.734	21.7
16	0.7	78.7	11.36	0.64	0.743	0.924	32.0
32	0.3	520.7	---	---	---	0.759	17.9
32	0.5	98.8	12.19	0.86	0.693	0.894	21.7
32	0.7	50.5	11.36	0.41	0.743	1.115	32.0

Figure 3 compares the simulated configurations in terms of SER and surface area, both of which are objectives to be minimized, while productivity is shown by the marker color. To identify designs that represent the best trade-offs between energy and material cost, a Pareto (non-dominance) analysis is performed in the two-dimensional objective space (SER – surface area). A case is classified as dominated if there is at least one other configuration that achieves an equal or lower SER and an equal or lower surface area simultaneously. Such cases are suboptimal under any weighting of these two objectives. In the given dataset, this screening removes only two configurations (crossed markers), indicating that most cases lie on or near the non-dominated set (Pareto front) and that the remaining designs reflect the trade-offs between reducing energy demand and reducing required surface area. Productivity is not used to define dominance in this analysis, but it provides additional information for interpreting the trade space.

The case $AR = 32$, $RR = 0.7$ achieves the lowest SER at the cost of the largest surface area. When the material cost is the limiting factor in the design of an adsorber for DAC, the Pareto-front representation indicates the increase in SER required to achieve a given reduction in surface area. For example, raising SER by 0.2 MJ/kg$_{CO2}$ (moving to $AR = 16$, $RR = 0.7$) allows the surface area to be reduced from 1.11 to 0.92 m^2. On the other hand, the case $AR = 4$, $RR = 0.3$ minimizes surface area but results in a very large SER due to a large pressure drop across the thicker bed. Increasing the bed aspect ratio from 4 to 8 lowers SER by 1 MJ/kg$_{CO2}$ while only slightly increasing the surface area.

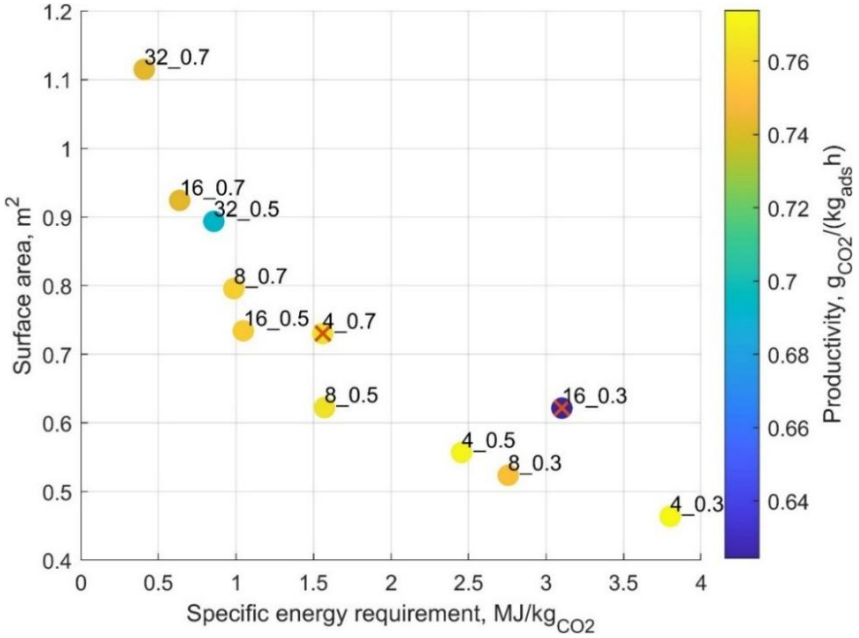

Figure 3. *Pareto analysis (case labels show the bed aspect ratio and the radius ratio of the studied configuration)*

Figure 4 presents the multi-criteria weighted-sum evaluation of the modeled configurations using all four performance metrics: specific energy requirement, productivity, surface area, and volume. Each metric was first mapped onto a dimensionless 0–1 scale, where 1 indicates the best-performing case and 0 indicates the worst within the set. A single composite score was then calculated for each configuration as a weighted sum of the four scaled scores. Figure 4 presents the resulting scores as five heatmaps corresponding to five weighting scenarios: an equal-weight baseline (0.25 assigned to each metric) and four additional scenarios in which one metric is emphasized (0.4) while the remaining three share the residual weight (0.2 each). This variation of weights concisely illustrates how the ranking responds to changes in the assumed priority of the evaluation criteria, and highlights configurations that remain highly ranked across multiple weighting assumptions as well as those that perform well only when a single criterion is favored.

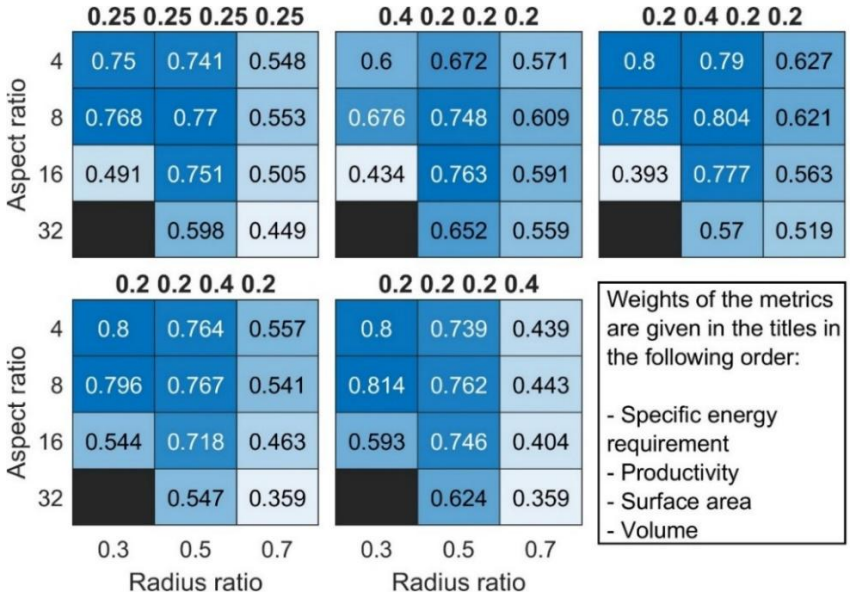

Figure 4. *Multi-criteria weighted-sum evaluation for five weighting scenarios*

The appropriate weight selection is the most sensitive aspect in the weighted-sum analysis, as many factors can affect the importance of different criteria. For example, higher electricity prices increase the relative importance of SER. In contrast, in regions with abundant low-cost renewable electricity, the weight of SER may decrease compared with the remaining criteria. Similarly, higher material cost can increase the emphasis on minimizing surface area, whereas site constraints and scale-up considerations affect the weight of the volume.

As can be seen from Figure 4, under the equal-weight scenario, configurations with lower aspect ratios and radius ratios are preferred. When the weight of surface area, productivity, or volume increases, the optimal design point shifts further toward lower AR and RR. However, when the weight of SER is increased, the case of $AR = 16$, $RR = 0.5$ becomes preferable. Higher RR is favored only when the weights assigned to the volume and surface area are small. Based on these results, SER should be treated as a central criterion while the other criteria can be treated together since increasing their weight produces a similar shift of the optimal design.

Figure 5 presents a similar weighted-sum evaluation but more focused on the importance of SER. It shows the same weighted composite score as a function of the weight of SER w_{SER} (from 0 to 1). The other three criteria share the residual weight evenly so that the sum of the weights equals 1. Each line on the graph corresponds to one configuration and shows its composite score as w_{SER} varies. For example, the case $AR = 4$, $RR = 0.3$ achieves the highest composite score when the weight of SER is close to zero, but as the importance of SER increases, the score decreases rapidly. In contrast, the case of $AR = 32$, $RR = 0.7$ becomes viable only when minimizing SER is the primary design objective. A vertical line drawn at $w_{SER} = 0.25$ reproduces the scores of each case for the first (equal-weight) scenario in Figure 4, and the vertical line at $w_{SER} = 0.4$ corresponds to the second scenario in Figure 4.

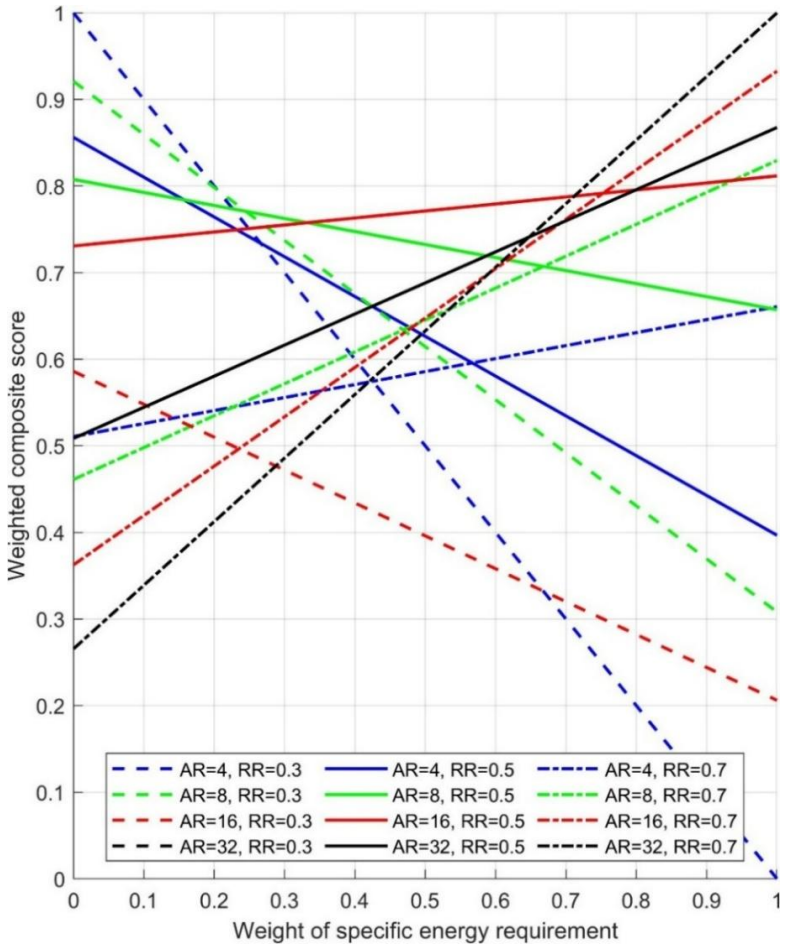

Figure 5. *Multi-criteria weighted-sum evaluation based on the weight of SER*

Figure 5 gives a broader overview of how the importance of SER can affect the design considerations. Low AR and RR cases perform well at lower weights of SER. As w_{SER} increases, intermediate values of AR and RR become preferred. Finally, if SER is the most important criterion, the design choices should shift toward high AR and RR values to minimize SER. The best adsorber configurations depending on w_{SER} are listed in Table 2. Overall, selecting $AR = 16$, $RR = 0.5$ maintains a high composite score across the entire range of w_{SER}, being outscored by other configurations only at the lowest and highest w_{SER}.

Table 2. *Preferable configuration for different weights of SER*

Range of w_{SER}	AR	RR
0 …0.21	4	0.3
0.21 … 0.24	8	0.3
0.24 … 0.33	8	0.5
0.33 … 0.71	16	0.5
0.71 … 1	32	0.7

4. Conclusion

Direct air capture plays an important role in achieving net-zero CO_2 emission targets. However, improving process efficiency and equipment design is needed to reduce the cost of DAC. In this work, a two-dimensional axisymmetric CFD model was developed to investigate the adsorption step of a solid-sorbent DAC process in a radial-flow adsorber. A geometric optimization was performed by varying the bed aspect ratio and radius ratio at a constant bed volume, and the configurations were evaluated using multi-criteria decision-making approaches. Specific energy requirement, productivity, surface area, and adsorber volume were calculated for each case and used as the main criteria for comparison.

The results showed that there is a clear trade-off between SER and the size of the adsorber: increasing the aspect ratio and radius ratio generally reduced SER, but also increased the adsorber's surface area and volume, causing higher material costs and space requirements. Productivity was reduced in cases with low RR and high AR because of the higher pressure drop in the axial channel and increased flow non-uniformity. Overall, the preferred configuration depended on the relative importance assigned to SER, but the case with $AR = 16$ and $RR = 0.5$ provided the most balanced performance across a wide range of weighting scenarios, whereas $AR = 32$, $RR = 0.7$ was preferable when minimizing SER was the main objective. These findings provide practical guidelines for the design of radial-flow adsorbers for DAC, while also showing that CFD, combined with multi-criteria decision-making, is an effective tool for geometric optimization and for understanding how adsorber geometry influences the performance of a DAC device under different energy, material, and space constraints.

Appendix A

Dimensions of the bed in all cases are presented in Table A.1.

Table A.1. *Dimensions of the bed in all cases*

AR	RR	Length L, m	Inner radius r, m	Outer radius R, m	Thickness, m
4	0.3	0.355	0.038	0.127	0.089
4	0.5	0.302	0.076	0.151	0.076
4	0.7	0.245	0.143	0.204	0.061
8	0.3	0.563	0.030	0.101	0.070
8	0.5	0.480	0.060	0.120	0.060
8	0.7	0.388	0.113	0.162	0.049
16	0.3	0.894	0.024	0.080	0.056
16	0.5	0.762	0.048	0.095	0.048
16	0.7	0.617	0.090	0.128	0.039
32	0.3	1.420	0.019	0.063	0.044
32	0.5	1.210	0.038	0.076	0.038
32	0.7	0.979	0.071	0.102	0.031

Nomenclature

A_{fs}	interfacial area density, 1/m
AR	bed aspect ratio
c_p	specific heat capacity, J/(kg K)
C_2	inertial resistance factor, 1/m

D_m mass diffusion coefficient, m^2/s

E specific total energy, J/kg

h specific enthalpy, J/kg

h_{fs} heat transfer coefficient for the fluid-solid interface, $W/(m^2\ K)$

ΔH adsorption enthalpy, J/mol

J diffusion flux, $kg/(m^2\ s)$

k thermal conductivity, W/(m K)

k_{LDF} mass transfer rate coefficient in the LDF model, 1/s

L length of the bed, m

m mass, kg

M molar mass, kg/mol

p pressure, Pa

q adsorption capacity, mol_{CO2}/kg_{ads}

q_{eq} equilibrium adsorption capacity, mol_{CO2}/kg_{ads}

Q volumetric flow rate, m^3/s

r radius of the inner channel, m

R outer radius of the bed, m

RR radius ratio

S_{CO2} CO_2 mass sink, $kg/(m^3\ s)$

S_E energy sink, $J/(m^3\ s)$

SER specific energy requirement, J/kg_{CO2}

t time, s

t_{sat} saturation time, s

T temperature, K

v velocity, m/s

V_{cell} volume of a computational cell, m^3

w_{SER} weight of SER

Y mass fraction

Greek symbols

α permeability, m^2

ε porosity

ρ density, kg/m^3

$\bar{\tau}$ stress tensor, Pa

Subscripts

ads adsorbent

$\mathrm{CO_2}$ carbon dioxide

f fluid

s solid

ref reference values

References

[1] IPCC, Climate Change 2023: Synthesis Report. Contribution of Working Groups I, II and III to the Sixth Assessment Report of the Intergovernmental Panel on Climate Change. Geneva, Switzerland: Intergovernmental Panel on Climate Change; 2023.

[2] IEA, Net Zero Roadmap: A Global Pathway to Keep the 1.5 °C Goal in Reach: 2023 Update. Paris, France: International Energy Agency; 2023.

[3] Smith S. M., Geden O., Gidden M. J., Lamb W. F., Nemet G. F., Minx J. C., Buck H., Burke J., Cox E., Edwards M. R., Fuss S., Johnstone I., Müller-Hansen F., Pongratz J., Probst B. S., Roe S., Schenuit F., Schulte I., Vaughan N. E., The State of Carbon Dioxide Removal 2024 – 2nd Edition; 2024.

[4] Zhu X., Xie W., Wu J., Miao Y., Xiang C., Chen C., Ge B., Gan Z., Yang F., Zhang M., O'Hare D., Li J., Ge T., Wang R., Recent advances in direct air capture by adsorption. Chemical Society Reviews 2022;51(15):6574-6651.

[5] Abdullatif Y., Sodiq A., Mir N., Bicer Y., Al-Ansari T., El-Naas M. H., Amhamed A. I., Emerging trends in direct air capture of CO2: a review of technology options targeting net-zero emissions. RSC Advances 2023;13(9):5687-5722.

[6] Shi X., Xiao H., Azarabadi H., Song J., Wu X., Chen X., Lackner K. S., Sorbents for the Direct Capture of CO2 from Ambient Air. Angewandte Chemie International Edition 2020;59(18):6984-7006.

[7] Jiang L., Liu W., Wang R. Q., Gonzalez-Diaz A., Rojas-Michaga M. F., Michailos S., Pourkashanian M., Zhang X. J., Font-Palma C., Sorption direct air capture with CO2 utilization. Progress in Energy and Combustion Science 2023;95:101069.

[8] Low M.-Y., Barton L. V., Pini R., Petit C., Analytical review of the current state of knowledge of adsorption materials and processes for direct air capture. Chemical Engineering Research and Design 2023;189:745-767.

[9] Wang J., Fu R., Wen S., Ning P., Helal M. H., Salem M. A., Xu B. B., El-Bahy Z. M., Huang M., Guo Z., Huang L., Wang Q., Progress and current challenges for CO2 capture materials from ambient air. Advanced Composites and Hybrid Materials 2022;5(4):2721-2759.

[10] Xu H., Yu L., Chong C., Wang F., A comprehensive review on direct air carbon capture (DAC) technology by adsorption: From fundamentals to applications. Energy Conversion and Management 2024;322:119119.

[11] IEA, Direct Air Capture 2022. France, Paris: International Energy Agency; 2022.

[12] Yu Q., Brilman W., A Radial Flow Contactor for Ambient Air CO2 Capture. Applied Sciences 2020;10(3):1080.

[13] Schellevis M., Jacobs T., Brilman W., CO2 Capture From Air in a Radial Flow Contactor: Batch or Continuous Operation? Frontiers in Chemical Engineering 2020;2:596555.

[14] Xu P., Wen J., Xin B., Huang W., Wang S., Comparison of Four Types of Vertical Radial-Flow Adsorbers Based on Binary Adsorption of CO2 and H2O. Chemical Engineering & Technology 2022;45(4):631-640.

[15] Abdullah M. Z., Qasim A., Parametric Analysis of Carbon Dioxide Adsorption on Nanoporous Activated Carbon Using Computational Approach. Procedia Engineering 2016;148:1416-1422.

[16] Ben-Mansour R., Basha M. N., Qasem N. A. A., Multicomponent and multi-dimensional modeling and simulation of adsorption-based carbon dioxide separation. Computers & Chemical Engineering 2017;99:255-270.

[17] Chen Q., Rosner F., Rao A., Samuelsen S., Jayaraman A., Alptekin G., Simulation of elevated temperature solid sorbent CO2 capture for pre-combustion applications using computational fluid dynamics. Applied Energy 2019;237:314-325.

[18] Chen S., Shi W. K., Yong J. Y., Zhuang Y., Lin Q. Y., Gao N., Zhang X. J., Jiang L., Numerical study on a structured packed adsorption bed for indoor direct air capture. Energy 2023;282:128801.

[19] Panagopoulos M., Lawson N. J., D'Alessandro D. M., Kearns E., Computational fluid dynamics analysis of a direct air capture filter system. In: Proceedings of the 34th Congress of the International Council of the Aeronautical Sciences; 2024 Sep 9-13; Florence, Italy.

[20] Sefidan A. M., Vepsäläinen J., CFD modelling of CO2 adsorption onto activated carbon: Insights into reactor and process design. Case Studies in Thermal Engineering 2025;75:107055.

[21] Li Y., Si H. Q., Wang H. B., Cheng X. H., Zhang P. H., Jia H. Y., Numerical Investigation of Integrated Design on Uniform Fluid Distribution for Radial Flow Adsorber. Theoretical Foundations of Chemical Engineering 2021;55(5):894-905.

[22] Zhang R., Wang Y., Yu X., Shen Y., Tang Z., Li W., Zhang D., Flow characteristics of air separation in VPSA process with radial flow adsorber. Powder Technology 2022;407:117672.

[23] Li S., Deng S., Zhao L., Zhao R., Lin M., Du Y., Lian Y., Mathematical modeling and numerical investigation of carbon capture by adsorption: Literature review and case study. Applied Energy 2018;221:437-449.